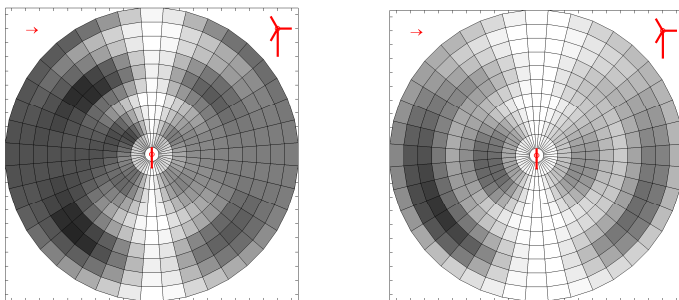




Executive summary

An explanation for enhanced amplitude modulation of wind turbine noise



Problem area

Modern large wind turbines normally produce a swishing noise with a sound level variation of a few decibels. However, in some cases periods of increased swish or thumping are reported. At present the source mechanism for this Enhanced Amplitude Modulation (EAM) is not clear.

Description of work

In order to identify potential causes for EAM, a simulation study was performed into the effects of wind shear on the sound of a modern large wind turbine. For this purpose, an existing turbine noise prediction model was extended to include an azimuth-dependent blade source distribution. Furthermore, a stall noise module was implemented.

Results and conclusions

The simulation results show that, as long as the flow over the blades is

attached, wind shear has practically no effect on amplitude modulation. However, strong wind shear can lead to local stall during the upper part of the revolution. This can yield noise characteristics which are very similar to those of EAM. Thus, it can be concluded that local stall is a plausible explanation for EAM. A sensitivity study was carried out to assess how critical the conditions for EAM are, and potential measures to prevent EAM are given. Apart from wind shear, other causes for a non-uniform inflow, such as yaw or topography, may also lead to local stall and EAM.

Applicability

The results from this study can be used to understand and reduce EAM, and to guide further research into this subject.

Report no.

NLR-CR-2011-071

Author(s)

S. Oerlemans

Report classification

COMPANY CONFIDENTIAL

Date

July 2011

Knowledge area(s)

Aeroacoustic and experimental aerodynamic research

Descriptor(s)

wind turbine noise

Nationaal Lucht- en Ruimtevaartlaboratorium, National Aerospace Laboratory NLR

Anthony Fokkerweg 2, 1059 CM Amsterdam,
P.O. Box 90502, 1006 BM Amsterdam, The Netherlands

Telephone +31 20 511 31 13, Fax +31 20 511 32 10, Web site: www.nlr.nl

UNCLASSIFIED



COMPANY CONFIDENTIAL

NLR-CR-2011-071

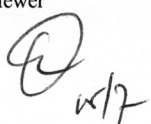

An explanation for enhanced amplitude modulation of wind turbine noise

S. Oerlemans

No part of this report may be reproduced and/or disclosed, in any form or by any means without the prior written permission of the owner.

Customer	RenewableUK
Contract number	2490258
Owner	RenewableUK
Division NLR	Aerospace Vehicles
Distribution	Limited
Classification of title	Unclassified
	July 2011

Approved by:

Author	Reviewer	Managing department
SO 15/7/11	 15/7	

COMPANY CONFIDENTIAL



Summary

Modern large wind turbines normally produce a swishing noise with a sound level variation of a few decibels. However, in some cases periods of increased swish or thumping are reported, denoted as Enhanced Amplitude Modulation (EAM). In order to identify potential causes for EAM, a simulation study was performed into the effects of wind shear on the sound characteristics of a representative modern large wind turbine. First, the effect of wind shear on the local blade flow conditions was determined. It was found that, for certain turbine operation conditions, strong wind shear can lead to local stall during the upper part of the revolution. In order to determine the corresponding sound characteristics, an existing turbine noise prediction model was extended to include an azimuth-dependent blade source distribution. Furthermore, a stall noise module was implemented. The simulation results show that, as long as the flow over the blades is attached, wind shear has practically no effect on the amplitude modulation. However, if local stall occurs, the resulting noise characteristics can be very similar to those of EAM. Thus, it can be concluded that local stall is a plausible explanation for EAM. A sensitivity study showed that the characteristics of wind shear induced amplitude modulation mainly depend on the size of the stall region (which in turn depends on blade design, turbine control system, operation conditions and wind shear) and on the stall noise behaviour of the airfoils used on the blade. Only for certain combinations of these parameters EAM will occur. The most obvious measure to prevent EAM is to prevent local stall on the blades, which can be achieved in several ways. Apart from wind shear, non-uniform inflow conditions may also be caused by e.g. yaw (wind veer), topography, large-scale turbulence, or the wake of other turbines. These effects may lead to local stall and as a consequence to EAM.



Contents

1	Introduction	7
2	Characteristics of enhanced amplitude modulation	9
2.1	Literature	9
2.2	Analysis of sound sample	11
3	Wind turbine noise prediction method	12
3.1	Simulation approach	12
3.2	Wind shear and blade flow conditions	13
3.3	Acoustic prediction method	15
4	Effect of wind shear on amplitude modulation	18
4.1	No wind shear: normal swish	18
4.2	Effect of wind shear for attached flow	19
4.3	Effect of local stall	20
4.4	Noise spectra	20
4.5	Sensitivity study	21
5	Conclusion	22
	References	24
	Figures	26



Nomenclature

Latin

2-D	Two-dimensional
3-D	Three-dimensional
a	Induction factor
A_i	Spectral shape function
EAM	Enhanced Amplitude Modulation
BPM	Airfoil noise prediction method by Brooks, Pope, Marcolini [20]
C	Airfoil chord
D_h, D_l	Directivity functions for high and low frequency, respectively
f	Frequency
L	Spanwise length of blade segment
m	Wind shear exponent
M	Mach number
SPL	Sound Pressure Level
OASPL	Overall Sound Pressure Level
r	Distance between source and observer
R	Rotor radius
Sr_i	Peak Strouhal number
St_i	Strouhal number $St = f \delta^* / U$
U	Flow speed
U_h	Wind speed at hub height
U_r	Rotational speed
U_w	Wind speed
U_z	Wind speed at height z
x, y, z	Turbine coordinate system (x in wind direction, z vertical)
x', y', z'	Airfoil coordinate system (x' along chord, y' along trailing edge)
z_h	Hub height

Greek

α	Angle of attack
α_{st}	Stall angle
δ_p^*	Trailing edge boundary layer displacement thickness on pressure side
δ_s^*	Trailing edge boundary layer displacement thickness on suction side
ζ	Angle between blade flow velocity and source-observer line
θ	Observer angle w.r.t. airfoil (see Figure 11)



μ	Sum of pitch angle and twist angle
ξ	Observer position w.r.t. wind turbine (0° is downwind, see Figure 15)
φ	Observer angle w.r.t. airfoil (see Figure 11)
ψ	Rotor azimuth angle (0° is 12 o'clock, see Figure 15)



1 Introduction

Wind is a clean, cheap, and inexhaustible source of energy. However, the noise from wind turbines constitutes an important hindrance for the widespread application of wind energy. The swishing character of the noise is often mentioned as an important factor explaining the relatively high annoyance, as compared to other sound sources of equal level (air or road traffic). Modern large wind turbines typically produce a swishing noise, i.e., a variation in the level of the broadband aerodynamic noise from the blades. This variation or modulation of the sound level occurs at the blade passing frequency, which is typically about 1 Hz. Normally, the peak-to-trough level variation (here denoted as ‘swish amplitude’) amounts to a few decibels. However, in some cases periods of increased swish or ‘thumping’ are reported, often referred to as Amplitude Modulation. Since normal swish is also an amplitude modulation of broadband blade noise, the term enhanced amplitude modulation or ‘EAM’ will be used in this report to denote increased swishing or thumping. The present study concerns a simulation study into potential causes for EAM. This study is part of a comprehensive research effort commissioned by RenewableUK [1,2]. The objective of this research effort is to identify the cause of EAM, and to develop an effective and reproducible measurement methodology and an associated dose-response relationship.

Normal blade swish can be explained as follows [3,4,5]. Under normal conditions (low wind shear), the blades produce a more or less constant amount of broadband noise during the complete revolution, which is caused by the turbulent airflow over the trailing edge of the blade (trailing edge noise). Due to directivity and convective amplification, this sound radiates mainly in the direction in which the blade is moving. In other words: you mainly hear the blade when it is coming towards you. For a nearby observer on the ground this means that most of the noise is produced when the blade moves downwards (roughly in the horizontal position for an upwind or downwind observer). Each time a blade passes this position, a swish is emitted. By the time the sound reaches the observer on the ground, the blades have already turned further. Therefore, it is sometimes suggested that the sound is produced when the blades pass the tower. However, acoustic source location measurements clearly demonstrate that the sound is produced around the 3 o’clock position (Figure 1).

The characteristics of normal swish can be analysed using a semi-analytical, semi-empirical wind turbine noise prediction method [5]. This frequency-domain prediction code only needs the blade geometry (airfoils, chord and twist distribution) and turbine operation conditions (wind speed, RPM, blade pitch) as input, and calculates the trailing edge noise from the blades. The effects of atmospheric turbulence, wind shear, and yaw are neglected, i.e., stationary and uniform inflow conditions are assumed. The prediction method was validated using acoustic data measured on a large circle around the turbine (radius 1.3 rotor diameters).



Good agreement was found between predictions and experiment, not only in terms of sound levels and spectra, but also with regard to turbine noise directivity and swish [5]. Calculated noise footprints show that, for observers more than a few rotor diameters away from the turbine, swish amplitudes up to about 5 dB may be expected in cross-wind directions, while in the up- and downwind direction no swish should be perceived (Figure 2). Close to the turbine, substantial swish (2-6 dB) is perceived in all directions. Similar trends were found using an alternative time-domain noise prediction method [6]. Note that in practice the perceived swish may reduce at large distance, due to a combination of the following factors: (1) inefficient sound propagation in cross-wind direction, (2) atmospheric absorption of high frequencies, and (3) the maximum sound level is below the background noise.

Thus, under typical conditions, trailing edge noise is the dominant noise source for modern large wind turbines, and normal swish can be explained using trailing edge noise directivity and convective amplification. However, in the case of EAM the reported noise characteristics are different (see Chapter 2): the variation in sound level is larger than 6 dB, and the level variations are also perceived at large distance, in upwind or downwind direction. In addition, there appears to be a change in the *character* of the noise, which becomes more impulsive and/or has increased low-frequency content. Several potential causes for EAM have been suggested, including wind shear, stall, yaw error, blade-tower interaction, inflow turbulence, and interference between different turbines. However, at present the mechanism is still not clear.

In this study, simulations will be carried out to investigate whether EAM can be explained by a non-uniform inflow. To facilitate the simulations, the existing prediction method [5] will be extended to include an azimuth-dependent blade noise source strength (azimuth is the angular position of the blade in the rotor plane). We will here focus on wind shear, but in practice non-uniform inflow conditions may also be caused by e.g. yaw, topography, large-scale turbulence or the wake of other turbines. Note that large-scale turbulence will only cause brief periods of non-uniform inflow. Wind shear results in an increased angle of attack during the upper part of the revolution and a lower angle of attack during the lower part of the revolution (Figure 3). A higher angle of attack leads to a thicker or even separated suction side boundary layer, which in turn yields a higher level and lower frequency of the trailing edge noise. Figure 3 also illustrates the effect of yaw (i.e., the deviation between the wind speed direction and the normal to the rotor plane). Yaw may occur due to *wind veer* - the variation in wind direction with height. Wind veer can reach values of 30° to 40° in the rotor plane of a wind turbine [7]. However, in practice wind veer is expected to have a smaller effect on the local angle of attack than wind shear. This is because wind shear directly affects the angle of attack through U_w , while yaw modifies U_w only by the cosine of the yaw



angle. For example, for $U_r/U_w = 7$ a yaw angle of 20° reduces the angle of attack by at most 0.8° , while a change in wind speed of 20% can change the angle of attack by $\pm 1.6^\circ$.

The structure of this report is as follows. In Chapter 2, we will first briefly review the characteristics of EAM, as guidance for the simulations. Next, the modified wind turbine noise prediction method is described in Chapter 3. The results of the simulations are presented and discussed in Chapter 4. Finally, the conclusions of this study are summarized in Chapter 5.

2 Characteristics of enhanced amplitude modulation

As mentioned above, normal swish, due to trailing edge noise directivity and convective amplification, causes peak-to-trough swish amplitudes up to 6 dB. For observers close to the turbine (less than two diameters away), substantial swish occurs in all directions, while at large distance (more than three diameters away) swish only occurs in cross-wind directions. In this chapter we will search the available literature for deviations from this pattern, since we are interested in EAM, which is by definition more ‘severe’ than normal swish. Thus, although the characteristics of EAM are unclear at this stage, EAM is here defined as an amplitude modulation which is stronger than the modulation predicted by the standard swish model described above*. Besides the noise characteristics, we will also try to find some clues about potential causes of EAM. In Section 2.1, we will briefly review the available literature. In Section 2.2, a sound sample will be analysed.

2.1 Literature

Extensive reviews of research into amplitude modulation of wind turbine noise were given by Moorhouse et al. [8], Bowdler [9] and Bullmore et al. [2]. In the following a short, more or less chronological, review will be given of the relevant observations.

Dunbabin [10] measured blade swish from a 34-m diameter pitch-controlled turbine using microphones on a 60-m diameter circle around the turbine. For constant conditions (yaw, power, pitch, wind speed), typical swish amplitudes of about 5 dB were found, but occasionally values of 10 dB were observed (in the 1 kHz and 2 kHz octave bands). Since the swishes did not occur at the same time on all microphones, it was concluded that the modulation was not due to the blades passing the tower. These results are well in line with the normal swish mechanism described above, except for the occasional 10-dB modulations, for which no explanation was given.

* The present definition of EAM is only intended to distinguish the different source mechanisms. It should not be interpreted as being a ‘threshold’ for *response* to amplitude modulation.



Van den Berg [11] measured the sound from a wind farm with seventeen 70-m diameter, pitch-controlled wind turbines. The measurement position was 750 m from the nearest turbine. The variation in A-weighted overall sound level was typically 2-3 dB, but during short periods values of 4-6 dB were measured. Due to the spatial extent of the wind farm, for some turbines the microphone was located in the downwind direction, but for other turbines it was located almost in the cross-wind direction. Therefore, the measured level variations may be partly explained by normal swish. Van den Berg investigated two other mechanisms to explain the modulation. First, he deduced that for extreme wind shear the trailing edge noise level may vary by up to 5 dB during one revolution, due to the change in angle of attack as explained above. However, it should be noted that due to summation of the noise from three blades, the *effective* sound level variation will be much smaller than this 5 dB. This can be illustrated by the fact that in Figure 1 the difference in source level between the upward and downward movement is about 12 dB, while the effective swish amplitude measured at the same location is only 2.5 dB [4]. This is also confirmed by the simulations by Boorsma et al. [12], who found a negligible influence of a standard wind profile on the (calculated) perceived trailing edge noise level variation. Figure 1 also illustrates that, at least in these measurements (unstable atmosphere), wind shear was not causing the swish, because then the source maximum should have been located around 12 o'clock.

The second mechanism investigated by van den Berg is synchronous running of different turbines. However, as noted before [9], such interaction between turbines cannot increase the level variation: if all turbines radiate swishes in phase (for a given observer position), the perceived modulation is the same as for a single turbine. If they are not in phase the level variation will be less. In summary, the observations by van den Berg may be explained by a combination of normal swish and extreme wind shear. The present study should give more insight into this possibility.

Moorhouse et al. [8] analyse EAM characteristics on the basis of complaints from residents for different sites. They mention variations in A-weighted sound levels of 3-5 dB and conclude that EAM occurs for specific wind directions, which occur between 7% and 25% of the time (for the four EAM sites analysed in detail). If for these wind directions the observers are located in the cross-wind direction with respect to the turbine(s), these results can be explained by normal swish. If the observers are in the upwind or downwind direction, another mechanism must be responsible for the level variations.

Di Napoli [13] measured the noise from a 1-MW pitch-controlled wind turbine on a downwind position at large distance. He reports overall level variations up to 5 dB, which were typically measured during periods of varying wind speed and rotational speed. In view of the downwind measurement position, these variations cannot be explained by normal swish. They may be related to off-design flow conditions on the blade (e.g. separated flow or stall), due to



the varying wind conditions. The effect of stall (due to strong wind shear) on the radiated noise will also be investigated in the present study.

Stigwood [14] reports level variations up to about 8 dB, both close to a single turbine and at large distance from a wind farm. These large variations cannot be explained by normal swish, and it is suggested that they are related to strong wind shear. He also notes that in case of EAM there is more low-frequency content in the sound. This could point to an increased boundary layer thickness at the trailing edge or even separated flow.

Vos et al. [15] measured the noise from a wind farm with seventeen 80-m diameter pitch-controlled turbines at distances between 200 m and 850 m. The sound level variations were 1-2 dB in 79% of the cases, 2-3 dB in 18% of the cases, and 3-4 dB in 1% of the cases. These findings appear to be in line with the characteristics of normal swish.

2.2 Analysis of sound sample

The characteristics of EAM are further investigated here by analysing a sound recording of about 25 s made by Bowdler [16]. It was measured about 50 m upwind from a 93-m diameter pitch-controlled wind turbine. The sample is particularly interesting because it contains the transition from normal swish to ‘thump’ (EAM). From subjective listening the transition occurs between 11 s and 13 s after the start of the sample. The complete sample sounds ‘aerodynamic’, i.e., the sound does not appear to be mechanical in nature.

The time history of the A-weighted overall sound level is shown in Figure 4. During the swish period (until 11 s) the average peak-to-trough level variation is 5.2 dB, which can be understood from the normal swish characteristics. However, during the EAM period (from 13 s onwards), the average level variation is 7.7 dB. If we look at the time difference between the minima and maxima (Figure 5), the RPM does not appear to be changing significantly during the change from swish to EAM. Furthermore, for both periods the average rise time (trough-to-peak) differs less than 10% from the average fall time (peak-to-trough), indicating that the modulations are not strongly asymmetric.

However, there appears to be a slight change in the *phase* of the swishes: whereas the time difference between consecutive minima and maxima is scattered around an average value of about 0.65 s in both periods, during the transition (around 12 s) it reaches 0.93 s. In the case of normal swish such a phase shift occurs when, due to a changing wind direction, the right hand side of the rotor plane (the descending blades) moves away from the upwind observer [5]. It is not clear if this was the case during the present measurement.

Finally, if we look at the average 1/3-octave band spectra for the swish period and the EAM period (Figure 6), we see that both have a broadband character, but that the EAM sound has much more low-frequency content. This is in line with the observations by Stigwood [14]



mentioned above, and suggests an increased boundary layer thickness or even separated flow, possibly due to an increased wind speed.

3 Wind turbine noise prediction method

Based on the EAM characteristics described in the previous chapter, we will now define the approach for the simulations (Section 3.1). The assumed wind shear characteristics and resulting blade flow conditions are discussed in Section 3.2. The acoustic prediction method is then described in Section 3.3.

3.1 Simulation approach

In the previous chapter we have seen that EAM is characterised by peak-to-trough level variations of more than 6 dB, and/or a substantial level variation at large distance in upwind or downwind direction. These observations cannot be explained by normal swish. As mentioned before, due to summation of the noise from three blades, we need a large variation in acoustic source strength during the revolution of the blade to explain these observations. As explained at the end of Chapter 1, trailing edge noise levels may be affected by variations in wind *speed* (shear) or wind *direction* (veer) over the rotor plane, or a combination of both. In the present study we will focus on wind shear, because the effect on angle of attack is expected to be stronger. Note that wind speed variations may also have other causes, such as large-scale atmospheric turbulence, topography, or the wake of other turbines. Wind shear will cause variations in angle of attack as a function of rotor azimuth, which will affect the trailing edge noise levels. However, as discussed in the previous chapter these noise level variations are probably too small to explain EAM. It is therefore also interesting to investigate whether *stall* may occur during part of the revolution (Figure 7). For stall-control wind turbines it is known that stall results in more noise [17]. For airfoils, the available literature suggests that stall results in a sudden increase of low-frequency noise [18,19,20,21]. This seems to be in line with the observations described in the previous chapter.

The noise simulations will be carried out for a representative large modern wind turbine with a tower height and rotor diameter of about 100 m. The turbine is pitch-controlled and has a rated power in the range of 2 MW. Based on the above considerations, the approach for the simulations is as follows. First, we will investigate which (extreme) wind shear conditions may occur in practice, and calculate the resulting angles of attack as a function of blade azimuth. This will enable us to assess whether local stall may occur. We will then calculate the trailing edge noise and/or stall noise for each blade segment, again as a function of blade azimuth. Finally, the noise from the three blades will be added and the total noise level will be computed



for different observer positions around the turbine, to estimate the perceived noise level variations. This will allow us to assess whether wind shear may explain the observed EAM characteristics.

The objective of this study is not to investigate in detail how and when stall occurs, or what the exact stall noise characteristics are. Rather, the goal is to assess (1) whether strong wind shear may lead to stall, and (2) if stall can lead to EAM. For this reason it is not very critical which turbine is used for the simulations, as long as it is representative for a large modern turbine. It should be noted that the effects of wind shear are modelled using engineering methods, which have not been validated by experiments yet.

3.2 Wind shear and blade flow conditions

In order to characterise the atmospheric wind shear we will apply the power law, which is used by many wind energy researchers [17]:

$$\frac{U_w(z)}{U_w(z_h)} = \left(\frac{z}{z_h} \right)^m \quad (1)$$

In this equation, U_w is the wind speed, m is the wind shear exponent, z is the height, and z_h is a reference height, for which here the hub height is taken. The wind shear exponent is a highly variable quantity. A low value indicates an unstable atmosphere with small variations in wind speed as a function of height, a high value indicates a stable atmosphere with high wind shear. Van den Berg [11] reports values for m between about 0.1 (unstable) and 0.6 (very stable) for a flat site in The Netherlands. The occurrence of these extreme values is a few percents of the time. Bowdler [7] showed that the wind shear exponent decreases with increasing wind speed. For a flat site in the UK, he found average values of 0.20 (daytime) and 0.43 (nighttime). In this study we will use values for m of 0 (no wind shear), 0.3 (stable), and 0.6 (very stable). The corresponding normalised wind speed in the rotor plane U_w/U_h , with U_h the wind speed at hub height, is shown in Figure 8.

In order to simulate the ‘worst case’ situation, we should use a (hub height) wind speed in the range where the turbine is most susceptible to stall, i.e., where the angles of attack are highest. This depends on the control system of the turbine, i.e., the variation of RPM and blade pitch angle as a function of wind speed. Variable-speed turbines typically increase the RPM (by adjusting generator torque) up to some wind speed, after which it remains constant. The pitch angle typically remains constant up to a certain wind speed, after which it is increased to control power. As illustrated in Figure 3, the angle of attack increases with increasing wind speed, but decreases with increasing RPM and increasing pitch angle. As a result the highest angles of attack, and therefore the highest susceptibility to stall, will occur at some intermediate wind



speed. The present simulations were done at a hub height wind speed of about 11 m/s, using the actual control settings of the present turbine.

For the aerodynamic and acoustic analysis the blade is divided into radial segments with a spanwise extent of about 1 m. As argued above, a full computation of the complex 3-D flow field around a rotating wind turbine blade in the presence of wind shear is beyond the scope of the present study. Therefore, we will assume local 2-D flow conditions for each blade segment. To assess whether stall can occur, we should check if the local angle of attack exceeds the stall angle α_{st} for the given airfoil. We will focus on the outer 40% of the blade, where all the noise is produced (aerodynamic noise is proportional to the 5th or 6th power of the local flow velocity). The angle of attack on each segment is calculated using the following equation:

$$\alpha = \tan^{-1} \left(\frac{(1-a)U_z}{U_r} \right) - \mu, \quad (2)$$

where U_z is the height-dependent wind speed, U_r the rotational speed of the blade element, and μ the sum of the blade pitch and the local twist of the blade segment. The induction factor a accounts for the fact that the wind is slowed down by the rotor. For an ideal rotor a equals 1/3, but we will here use a slightly lower value a_0 , because for a uniform inflow the resulting angles of attack on the outer 40% of the blade agree within 0.1° with those calculated using a more advanced blade element momentum method [22]. To account for induced downwash due to the tip vortex, the angle of attack for the outer blade element is reduced by 1°.

If for a given blade segment stall occurs during part of the revolution, the local lift production decreases. As a result the local induction factor decreases and the angle of attack calculated using Eq. (2) increases. For a typical airfoil, stall results in a lift reduction of about 25% to 50%. Assuming that the lift is proportional to $a(1-a)$ [17], the local induction factor will reduce by about 50% in the case of stall. Thus, the flow state on a given blade segment depends on the local wind speed as follows: for low wind speeds the flow is always attached and for high wind speeds the flow is always stalled. For intermediate wind speeds two solutions exist: the flow may be either attached ($\alpha < \alpha_{st}$ for $a = a_0$) or stalled ($\alpha > \alpha_{st}$ for $a = a_0/2$).

The locations in the rotor plane where the angle of attack may exceed the stall angle are shown in Figure 9 for two values of the wind shear coefficient. The plots show that stall can occur for a substantial part of the rotor plane. As expected the stall region increases with increasing shear factor. It should be noted that these calculations were done using the ‘stall value’ $a = a_0/2$ for the induction factor. If attached flow is assumed, with $a = a_0$, the angle of attack is always smaller than α_{st} for the conditions in Figure 9. This means that both flow states (attached flow and stalled flow) are possible for the indicated locations. In the following we will



assess both situations. Stall hysteresis or dynamic stall effects (delay of stall due to rapid α increase and vice versa) are not taken into account.

In order to calculate the trailing edge noise, we need to know the boundary layer displacement thickness at the trailing edge of each blade segment. For the present conditions the Reynolds number on the outer 40% of the blade ranges between about 3 and 6 millions, and the angle of attack between $\alpha_{st} - 5$ and $\alpha_{st} + 2$. For these conditions the dependence on Reynolds number is small, and we can estimate the trailing edge boundary layer thickness on the suction and pressure side (for attached flow) using the relations shown in Figure 10, where δ^* is the displacement thickness, C is the airfoil chord and α the angle of attack. These approximations are based on calculations with the RFOIL airfoil design and analysis code [23] for the present airfoil.

3.3 Acoustic prediction method

This section describes the acoustic prediction method for attached flow and stalled flow. Furthermore, it is explained how the resulting blade noise spectra are transferred to the wind turbine noise footprint.

3.3.1 Trailing edge noise for attached flow

For attached flow, the trailing edge noise from each blade segment is calculated with the method described and validated in Ref. 5. Using the local Reynolds number, angle of attack and boundary layer displacement thickness from the previous section as input, the source spectrum for each radial blade segment is calculated using the 2D semi-empirical trailing edge noise prediction code developed by Brooks, Pope and Marcolini [20]. In this code, which is based on acoustic and aerodynamic wind tunnel measurements on NACA0012 airfoils, the total trailing edge source strength due to the turbulent boundary layer is the sum of three contributions of the following form:

$$SPL_i = 10 \log \left(\frac{\delta_i^* M^5 L}{r^2} \right) + A_i \left(\frac{St_i}{Sr_i} \right) + K_i, \quad (3)$$

where δ^* is the displacement thickness, M the Mach number, L the span of the blade segment, r the distance to the observer, and K an empirical constant which depends on the Mach and Reynolds numbers. The function A describes the spectral shape as a function of the ratio between the Strouhal number $St = f \delta^* / U$ (with U the local flow speed) and the empirical peak Strouhal number Sr . The three contributions (here denoted by the index i) are the pressure side boundary layer, the suction side boundary layer, and an additional contribution to account for nonzero angle of attack. Eq. (3) basically states that trailing edge noise is



proportional to the boundary layer thickness (which is a measure for the turbulence correlation scale) and the fifth power of the flow speed. The boundary layer thickness for the different blade segments of the present wind turbine blade is calculated using the approximation described in the previous section. To account for directivity and convective amplification a smoothed version of the trailing edge noise directivity function is used [5]:

$$D_h = \frac{\left[2 \sin^2(\theta/2) \sin^2 \phi \right]_s}{(1 - M \cos \zeta)^4}, \quad (4)$$

where the subscript s indicates the smoothing, θ and ϕ are defined in Figure 11, ζ is the angle between the blade flow velocity and the source-observer line, and M is the Mach number. The numerator in Eq. (4) describes the trailing edge noise directivity, and indicates that the noise is mainly radiated towards of the leading edge. The characteristics of this function are shown in Figure 12. The denominator represents the convective amplification factor for trailing edge noise, and indicates that the source amplitude increases when the source is moving towards the observer. The Doppler *frequency* shift is accounted for by calculating for each source frequency the Doppler-shifted frequency at the observer position, and redistributing the acoustic energy over the appropriate frequency bands.

3.3.2 Stall noise

For stalled flow, the prediction method should reflect the characteristics mentioned in literature [18,19,21]: a sudden increase in noise accompanied by a shift to lower frequencies. Such a noise increase, occurring only for part of the revolution, may explain the EAM observations mentioned above (level variations exceeding 6 dB and/or a substantial level variation at large distance in upwind or downwind direction). The increase in sound level for stalled flow can be physically understood from the larger turbulence length scales, the larger coherence length, and the higher turbulence intensity (as compared to attached flow). In Ref. [19] stall was found to result in a 10 dB increase in broadband noise. In Ref. [18] the noise increase due to stall appeared to be somewhat lower than 10 dB, but in Ref. [21] noise increases up to 20 dB (light stall) or 30 dB (deep stall) were found in a certain frequency range. All in all, it seems reasonable to assume an increase of 10 dB in overall sound level, although the actual value may depend on the airfoil. Thus, the prediction method should exhibit a sudden noise increase of about 10 dB when stall occurs.

The shift to lower frequencies for stall noise can be physically understood from the larger turbulence length scales. In Ref. [21] the front projection of the airfoil ($C \sin \alpha$) was used as the relevant length scale, and the stall noise spectrum was found to peak at a Strouhal number of about 0.3. For attached flow (see previous section), the trailing edge noise spectrum



peaks at a Strouhal number $St = f\delta^*/U$ of about 0.15. Since for the present conditions the attached boundary layer thickness δ_s^* is about four times smaller than $C \sin \alpha$, this implies that the peak frequency is roughly halved when stall occurs. This change in peak frequency should be captured by the prediction method.

The Brooks, Pope and Marcolini or ‘BPM’ model [20], which is used in the present study to calculate the trailing edge noise for attached flow (see previous section), also contains a module for noise from a stalled airfoil. In this module Eq. (3) is still used, but for $\alpha > \alpha_{st}$ only the $i = 3$ term is retained, and the width of the noise spectrum is increased. The peak level and frequency are controlled by the displacement thickness δ_s^* of the stalled flow. In order to capture the desired characteristics for stall noise, for the present application the BPM module is implemented in the following way. First, it is assumed that δ_s^* increases by a factor of two when stall occurs. This yields the desired reduction in peak frequency by a factor of two, as argued above, and an increase in level of about 3 dB. Second, 7 dB is added to the spectral levels calculated using the BPM code, in order to obtain the desired 10 dB overall noise increase. The resulting blade noise spectra as a function of angle of attack, for an airfoil on the outer part of the blade, are shown in Figure 13 and Figure 14. For $\alpha < \alpha_{st}$ (attached flow), the spectrum consists of two ‘humps’ representing the contributions from the suction and pressure side of the airfoil. As expected, the low-frequency (suction side) hump increases in level and decreases in frequency for increasing angle of attack. At the stall angle, the width of the spectrum can be seen to increase. Moreover, the peak frequency is reduced and the level increases substantially. As a result, the overall sound level increases by about 10 dB at the stall angle (Figure 14).

As explained above, the dominant frequencies for stall noise are lower than for trailing edge noise, due to the larger turbulence length scale. As a result the acoustic wavelength becomes of the same order as the airfoil chord. Thus, for stall noise the directivity function of a compact dipole is used:

$$D_i = \frac{\sin^2 \theta \sin^2 \phi}{(1 - M \cos \zeta)^4}. \tag{5}$$

This function corresponds to the low-frequency directivity function used for stall noise in the BPM model. The numerator indicates that the noise is mainly radiated in the direction perpendicular to the plane of the airfoil. The characteristics of this function are shown in Figure 12. The denominator is the same as for the trailing edge noise directivity function in Eq. (4), and indicates that the source amplitude increases when the source is moving towards the observer. The Doppler *frequency* shift is calculated in the same way as for trailing edge noise.



3.3.3 Noise footprints

The time-dependent noise footprints of the turbine are calculated in the same way as described in Ref. [5], except that the blade noise source strength now depends on azimuth. Three blades are modeled at 120° from each other and the azimuth-dependent radial source distribution for each blade is calculated as described in the previous sections. For each rotor azimuth the contribution of each blade segment to the sound level at a certain observer position is calculated, using the directivity functions of Eqs. (4) and (5). Note that for a given *arrival* time, the *emission* time (i.e., emission azimuth) is generally different for the different blade elements. By plotting the total sound level at different observer positions for a fixed observer time, the instantaneous noise footprint is obtained. It should be noted that the prediction model focuses on the *sources* of wind turbine noise, which means that propagation effects, such as sound refraction due to wind shear, are not included.

4 Effect of wind shear on amplitude modulation

In this chapter the results of the simulations will be presented and discussed. In order to assess the effect of wind shear on amplitude modulation, simulations were carried out for the following five cases:

1. No wind shear ($m = 0$), attached flow;
2. Stable atmosphere ($m = 0.3$), attached flow;
3. Very stable atmosphere ($m = 0.6$), attached flow;
4. Stable atmosphere ($m = 0.3$), local stall;
5. Very stable atmosphere ($m = 0.6$), local stall.

As explained in Section 3.2, for the cases with wind shear both attached and stalled flow may occur for the locations indicated in Figure 9. Therefore both situations are simulated. The structure of this chapter is as follows. First, the simulation results for the reference case (no wind shear) are presented in Section 4.1. Next, in Section 4.2 the effect of wind shear on amplitude modulation will be assessed for attached flow (Cases 2-3). Then, in Section 4.3 the effect of local stall will be investigated (Cases 4-5). Finally, the sensitivity of the simulation results to different model parameters will be studied in Section 4.5. The rotor azimuth angle ψ and the observer angle ξ are defined in Figure 15. We will focus on the results at large distance, because these are most relevant for noise pollution.

4.1 No wind shear: normal swish

As a ‘normal swish’ reference, the simulation results for Case 1 (no wind shear) are presented in Figure 16. The upper row shows instantaneous turbine noise footprints (top view) for four



different rotor azimuth angles, up to a distance of ten times the rotor diameter. The turbine is located at the center of the footprint, and the wind goes from left to right. The rotor azimuth (as seen from an upwind position) at observer time is indicated in the upper right corner of each footprint. In order to limit the range of the dB scale and show the level variations more clearly, the sound levels are normalized using the horizontal distance r_h to the turbine:

$SPL_{norm} = SPL + 20 \log r_h$. In this way the levels at a given distance can still be directly compared. The sound levels are integrated between 100 Hz and 5 kHz and are given in dBA. The footprints show two waves of increased sound level, one in each cross-wind direction, which start close to the turbine at $\psi = 90^\circ$ and propagate outward with the speed of sound. The wave on the side of the descending blade is generated when the blade is around 1 o'clock, while the wave on the side of the ascending blade is generated when the blade is around 6 o'clock. After $\psi = 180^\circ$ the cycle repeats and both waves can be seen to propagate further to the edge of the footprints.

Due to the passage of these sound waves from the blades, the noise levels in the crosswind directions vary significantly, while in the upwind and downwind directions the levels are practically constant at large distances. This is illustrated in the middle row of Figure 16, which shows the average and swish (level variation) footprints for a complete revolution. Note that these footprints are very similar to those in Figure 2, which suggests that the general pattern does not depend strongly on turbine or operation details. The footprints in Figure 16 show that for both cross-wind directions, the *average* level is lower than in the up- and downwind directions, but the *variation* in level is larger. The patterns do not change significantly beyond a distance of a few rotor diameters. The sound characteristics at large distance, which are most relevant for noise annoyance, are quantified in the lower row of Figure 16. Note that in the time histories, the vertical ticks are spaced at 6 dB. It can be seen that even at a large distance, trailing edge noise directivity and convective amplification may cause swish amplitudes up to about 5 dB in the cross-wind directions. In the upwind and downwind directions the swish is practically zero. The slightly higher level in the upwind direction is due to the fact that the blade flow vector U is tilted towards the downwind direction (Figure 3), which affects the convective amplification factor in the denominator of Eq. (4).

4.2 Effect of wind shear for attached flow

The results for Cases 2 and 3 ($m = 0.3$ and $m = 0.6$, attached flow) are presented in Figure 17 and Figure 18. In general the sound characteristics are very similar to those for Case 1, except that the waves on the side of the descending blade have a slightly higher level than those on the side of the ascending blade. This is because the blades produce more noise around 12 o'clock than around 6 o'clock, due to the higher wind speed at larger height. However, the swish is still not higher than about 5 dB in the cross-wind directions, and practically zero in the upwind and



downwind directions. Thus, it appears that EAM cannot be explained by wind shear, as long as the flow is still attached and no stall occurs.

4.3 Effect of local stall

The results for Cases 4 and 5 ($m = 0.3$ and $m = 0.6$, local stall) are presented in Figure 19 and Figure 20. The stall locations for both cases are shown in Figure 9. The sound characteristics clearly differ from the cases without stall. Most of the noise is produced during the upper part of the revolution, where stall occurs. Due to the different directivity function for stall noise, sound waves are radiated in the upwind and downwind direction. Due to the convective amplification factor in the denominator of Eq. (5), the noise level on the side of the descending blade is slightly higher than on the side of the ascending blade. For $m = 0.3$, where the stall region is smaller than for $m = 0.6$, the sudden noise increase during part of the revolution causes substantial amplitude modulation (about 3 dB) in the upwind and downwind directions at large distance (see Figure 21). This modulation is not found for the cases without stall and seems to be in line with the EAM observations described in Chapter 2. Moreover, closer to the turbine amplitude modulations exceeding 6 dB are observed in the cross-wind direction (Figure 22). These high modulation amplitudes are not found for the cases without stall. In Figure 20, the time history for $\xi = 270^\circ$ shows a complex modulation pattern. This is probably due to different blades sequentially leaving and entering the stall region. Note that the *average* level in this cross-wind direction is much lower than in other directions.

The above results show that local stall can yield noise characteristics which are very similar to the EAM characteristics mentioned in Chapter 2: substantial swish at large distance in upwind and downwind directions, level variations exceeding 6 dB, and more low-frequency content. Thus, local stall is a plausible explanation for EAM. In Section 4.5 a sensitivity study will be carried out to investigate how critical the conditions for EAM are.

4.4 Noise spectra

The noise spectra for Cases 1-5, as perceived at large distance in upwind and downwind directions and averaged over a complete revolution, are presented in Figure 23 (normalised absolute levels). It can be seen that, as long as the flow remains attached, wind shear has almost no effect on the average spectra. This is because the small increase in angle of attack for the upper part of the revolution (about 1.5° at most) is compensated by a reduction in angle of attack for the lower part of the revolution. The noise increase in case of local stall (Cases 4 and 5) is clearly visible. Although the peak frequency remains practically the same as for attached flow (due to A-weighting, see Figure 13), the largest noise increase occurs at the lower frequencies.



The corresponding spectra for the cross-wind directions are shown in Figure 24. It should be noted that the average sound level in the cross-wind directions is much lower than in the upwind and downwind directions (see Figure 16 to Figure 20). For $\xi = 90^\circ$ most of the perceived noise is produced around 6 o'clock. For attached flow (Cases 1-3) the noise level reduces with increasing shear factor, because the wind speed at 6 o'clock reduces and as a result the angle of attack and boundary layer thickness reduce as well. Local stall (Cases 4 and 5) results in a slight noise increase with respect to the corresponding attached flow cases. For $\xi = 270^\circ$ most of the perceived noise is produced around 1 o'clock. Now the noise level for attached flow increases with increasing shear factor, due to the increased wind speed at 1 o'clock. Interestingly, the perceived levels decrease in case of local stall. This is because the trailing edge noise which was radiated from around 1 o'clock in the attached flow cases, is now replaced by stall noise, which is radiated mainly in the upwind and downwind directions.

Instantaneous spectra for the downstream observer position are shown in Figure 25. It can be seen that the modulation has a broader spectrum in the peak than in the trough. This is because the peak is dominated by stall noise and the trough by trailing edge noise from the attached flow. The average noise spectra for observer positions close to the turbine (at one rotor diameter) are similar to those at large distance (Figure 26). The effect of local stall is less pronounced than at large distance (Figure 23), because close to the turbine most of the noise is produced around the 3 o'clock position, where trailing edge noise is dominant.

4.5 Sensitivity study

In this section we will investigate the sensitivity of the simulation results to different model parameters. Throughout this section, Case 4 ($m = 0.3$, local stall) will be used as a reference, since this case showed the largest modulation in upwind and downwind directions at large distance. We will focus on the modulation amplitude at large distance. The effect of the wind shear exponent m is shown in Figure 27. The general trend is the same for different values of m , but the highest modulation amplitude in upwind and downwind direction (about 4 dB) is found for $m = 0.4$. For smaller m the smaller stall region results in less noise increase and therefore less modulation, while for higher m the larger stall region gives less modulation due to the summation of the noise from the three blades.

The effect of the blade pitch angle is shown in Figure 28. It can be seen that for a small decrease in pitch angle (larger angle of attack) the characteristics remain similar to the reference case. However, if the pitch angle is increased, the stall region becomes smaller and the modulation amplitude becomes similar to that for attached flow (see Figure 17). Thus, the effect of blade pitch on amplitude modulation is mainly determined by the size of the stall region.

Finally, the influence of the stall noise level increase is investigated. As explained in Section 3.3.2, the prediction model assumes a noise increase of about 10 dB when stall occurs



(see Figure 13 and Figure 14). It was already mentioned that the level increases reported in literature vary, and that the actual value may depend on the airfoil. The effect of a 3 dB change in this stall noise level increase is shown in Figure 29. As expected, the modulation amplitude increases with increasing stall noise level increase, although the trends remain similar. Thus, the magnitude of the modulation amplitude strongly depends on the stall noise level increase of the airfoil. This means that, in order to predict an accurate quantitative value of the amplitude modulation for a given turbine, detailed information about the stall noise behaviour of the relevant airfoils is needed.

In summary, it can be concluded that the characteristics of wind shear induced amplitude modulation mainly depend on the size of the stall region (which in turn depends on blade design, turbine control system, operation conditions and wind shear) and on the stall noise behaviour of the airfoils used on the blade.

5 Conclusion

Modern large wind turbines normally produce a swishing noise with a sound level variation of a few decibels. However, in some cases periods of increased swish or thumping are reported, here denoted as as Enhanced Amplitude Modulation (EAM). The characteristics of EAM were investigated by means of a literature study and by analysis of a sound sample. It was concluded that EAM can be characterised by sound level variations of more than 6 dB and/or substantial level variations at large distance in upwind or downwind direction, often accompanied by more low-frequency content in the sound.

In order to identify potential causes for EAM, a simulation study was performed into the effects of wind shear on the sound characteristics of a representative modern large wind turbine. First, the effect of wind shear on the local blade flow conditions was determined. It was found that, for certain operation conditions (where the blades are most susceptible to stall), strong wind shear can lead to local stall during the upper part of the revolution. Next, in order to determine the corresponding sound characteristics, an existing turbine noise prediction model was extended to include an azimuth-dependent blade source distribution. Furthermore, a stall noise module was implemented. It should be noted that the effects of wind shear were modelled using engineering methods, which have not been validated by experiments yet. The simulation results show that, as long as the flow over the blades is attached, wind shear has practically no effect on the amplitude modulation. However, if local stall occurs, the resulting noise characteristics can be very similar to the EAM characteristics mentioned above, depending on the size of the stall region. Thus, it can be concluded that local stall is a plausible explanation for EAM.



In order to assess how critical the conditions for EAM are, a sensitivity study was carried out. This study showed that the occurrence of EAM for this specific turbine strongly depends on wind shear, blade pitch, and the assumed stall noise level increase. More generally, it can be concluded that the characteristics of wind shear induced amplitude modulation mainly depend on the size of the stall region (which in turn depends on blade design, turbine control system, operation conditions and wind shear) and on the stall noise behaviour of the airfoils used on the blade. Only for certain combinations of these parameters EAM will occur. The most obvious measure to prevent EAM is to prevent local stall on the blades. An increase in the stall margin may be achieved by operating the blades at a lower angle of attack or by using airfoils with a high stall angle. A practical implementation for existing turbines may be to increase the blade pitch angle in case of strong wind shear.

Finally, it should be noted that, apart from wind shear, (temporary) non-uniform inflow conditions may also be caused by e.g. yaw (wind veer), topography, large-scale turbulence, or the wake of other turbines. These effects may lead to local stall and as a consequence to EAM. Thus, for future experimental research into EAM, it is recommended to focus not only on the sound characteristics, but to monitor as much as possible also the turbine operation parameters and meteorological conditions. A convenient method for detecting local stall could be the use of stall-flags [24,25].



References

- [1] J. Bass, D. Bowdler, M. McCaffery, G. Grimes, Fundamental research in Amplitude Modulation – a project by RenewableUK, Proceedings of Wind Turbine Noise 2011, 2011.
- [2] A. Bullmore, M. Jiggins, M. Cand, M. Smith, S. von Hünenbein, R. Davis, Wind turbine amplitude modulation: research to improve understanding as to its cause & effect, Proceedings of Wind Turbine Noise 2011, 2011.
- [3] S. Oerlemans, P. Sijtsma, B. Méndez López, Location and quantification of noise sources on a wind turbine, Journal of Sound and Vibration 299, 869-883, 2007[†].
- [4] S. Oerlemans, M. Fisher, T. Maeder, K. Kögler, Reduction of wind turbine noise using optimized airfoils and trailing-edge serrations, AIAA Journal Vol. 47, No. 6, 2009[†].
- [5] S. Oerlemans, J.G. Schepers, Prediction of wind turbine noise and validation against experiment, International Journal of Aeroacoustics, Vol. 8, No. 6, 2009[†].
- [6] S. Lee, S. Lee, S. Lee, Time domain modeling of aerodynamic noise from wind turbines, Proceedings of Wind Turbine Noise 2011, 2011.
- [7] D. Bowdler, Wind shear and its effect on noise assessment, Proceedings of Wind Turbine Noise 2009, 2009.
- [8] A. Moorhouse, M. Hayes, S. von Hünenbein, B. Piper, M. Adams, Research into aerodynamic modulation of wind turbine noise: final report, University of Salford, July 2007.
- [9] D. Bowdler, Amplitude modulation of wind turbine noise, Acoustics Bulletin of the Institute of Acoustics (UK), Vol. 33, No. 4, July/August 2008.
- [10] P. Dunbabin, An investigation of blade swish from wind turbines, Proceedings of Internoise 96, 1996.
- [11] G. P. van den Berg, The sounds of high winds, PhD thesis University of Groningen, The Netherlands, 2006.
- [12] K. Boorsma, J. G. Schepers, Enhanced wind turbine noise prediction tool SILANT, Proceedings of Wind Turbine Noise 2011, 2011.
- [13] C. Di Napoli, Wind turbine noise in a small and quiet community in Finland, Proceedings of Wind Turbine Noise 2009, 2009.
- [14] M. Stigwood, DenBrookMASPOE90625, June 2009.
- [15] J. Vos, M. M. J. Houben, Analysis of wind turbine noise recordings (in Dutch), TNO report TNO-DV 2010 C014, 2010.

[†] Part of: S. Oerlemans, Detection of aeroacoustic sound sources on aircraft and wind turbines, PhD thesis University of Twente, The Netherlands, 2009 (<http://doc.utwente.nl/67363/>).



- [16] www.dickbowdler.co.uk.
- [17] J.F. Manwell, J.G. McGowan, A.L. Rogers, Wind energy explained – Theory, design and application, John Wiley & Sons, 2002.
- [18] R. W. Paterson, R. K. Amiet, C. L. Munch, Isolated airfoil – tip vortex interaction noise, AIAA paper 74-194, 1974.
- [19] M. R. Fink, D. A. Bailey, Airframe noise reduction studies and clean-airframe noise investigation, NASA-CR-159311, 1980.
- [20] T. F. Brooks, D. S. Pope, M. A. Marcolini, Airfoil self-noise and prediction, NASA-RP-1218, 1989.
- [21] S. Moreau, M. Roger, J. Christophe, Flow features and self-noise of airfoils near stall or in stall, AIAA paper 2009-3198, 2009.
- [22] B. H. Bulder, S. A. M. Barhorst, J. G. Schepers, F. Hagg, Theory and user's manual BLADOPT, ECN-C-01-011, Energy Research Centre of the Netherlands ECN, 2001.
- [23] B. Montgomerie, A. Brand, J. Bosschers, R. van Rooij, Three-dimensional effects in stall, ECN-C-96-079, Energy Research Center of the Netherlands ECN, 1997.
- [24] G. P. Corten, H. F. Veldkamp, Insects cause double stall, European Wind Energy Conference, Copenhagen, 2001.
- [25] G. P. Corten, H. F. Veldkamp, Insects can halve wind-turbine power, Nature, Vol. 412, 2001.

Figures



Figure 1: Noise source distribution in the rotor plane of a modern large wind turbine, measured about one rotor diameter upwind from the turbine. The source distribution is averaged over many revolutions. The range of the colour scale is 12 dB. Practically all noise is produced by the outer part of the blades (not the very tip) during the downward part of the revolution.

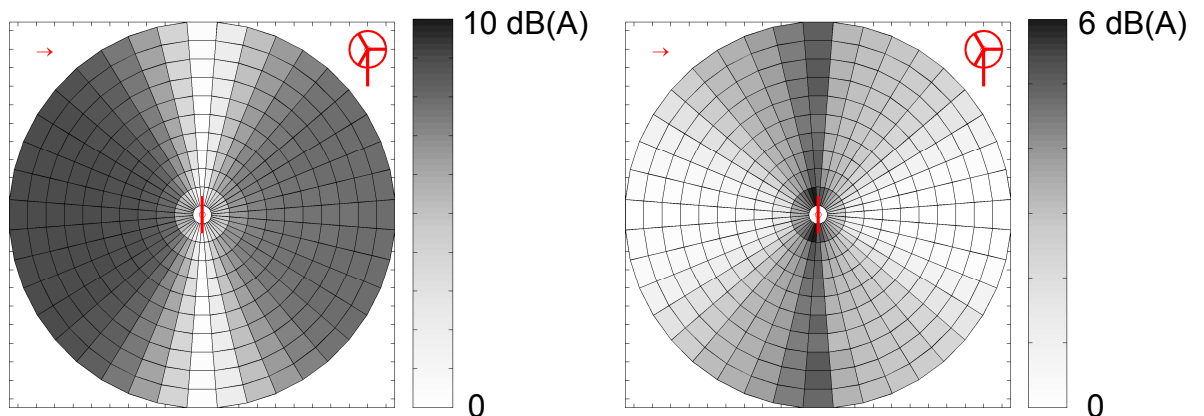


Figure 2: Footprints of the average sound level (left) and the sound level variation (right) during a revolution [5]. The turbine is located at the centre of the plot (top view), and the wind goes from left to right. The radius of the plotted area equals 10 rotor diameters. The figure shows that, for an observer more than a few rotor diameters away, the average levels are highest in the upwind and downwind directions, but the variations in level are largest in the cross-wind directions. Close to the turbine, substantial swish is perceived in all directions.

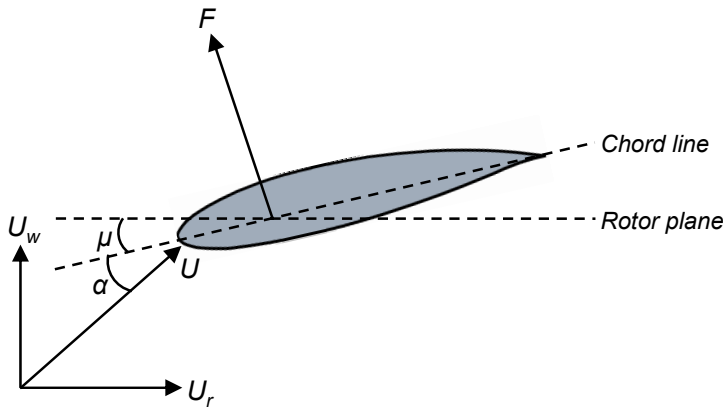


Figure 3: Airfoil with definition of flow angles. U_w is the wind speed, U_r is the rotational speed, μ is the pitch angle and α is the angle of attack. F is the force on the blade. Close to the blade tip U_r is usually roughly seven times higher than U_w . An increase in wind speed leads to a higher angle of attack.

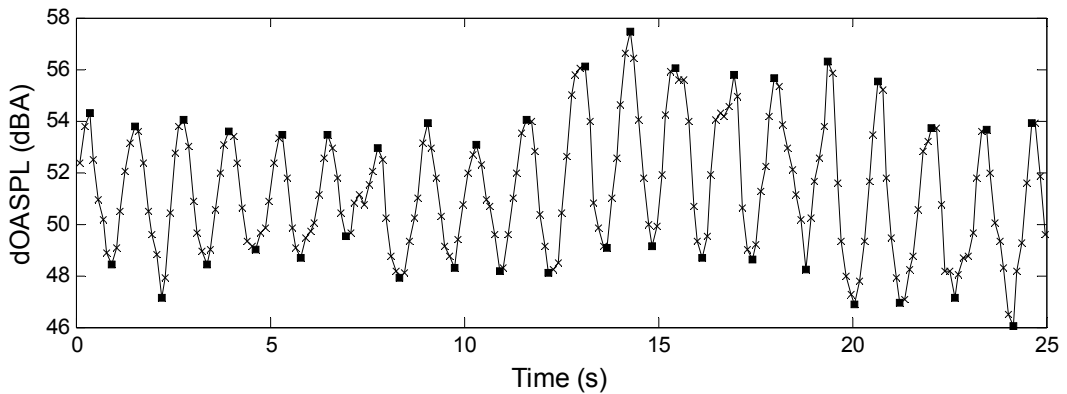


Figure 4: Time history of A-weighted overall sound level as a function of time (absolute levels not meaningful). The transition between normal swish and EAM occurs between 11 s and 13 s. The crosses indicate the instantaneous levels (averaged over 0.23 s), the squares indicate the maxima and minima.

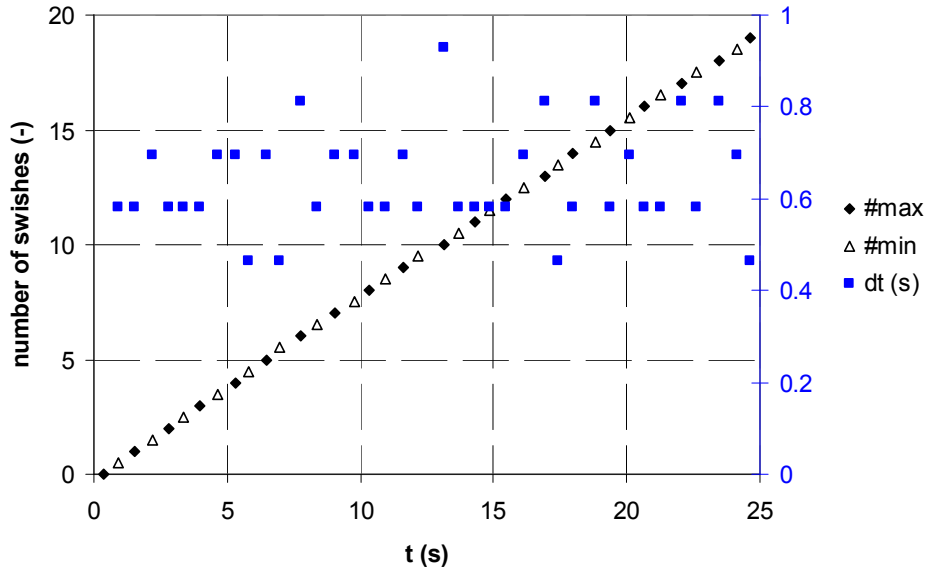


Figure 5: Number of maxima and minima as a function of time (left axis). The blue markers (right axis) indicate the time difference between consecutive minima and maxima.

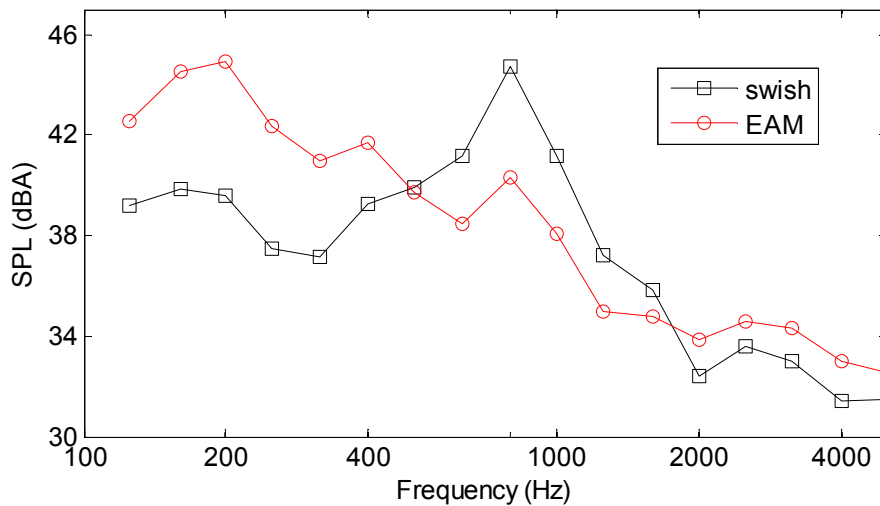


Figure 6: Average spectra for swish period and EAM period (absolute levels not meaningful). The EAM sound has much more low-frequency content than the swishing sound.

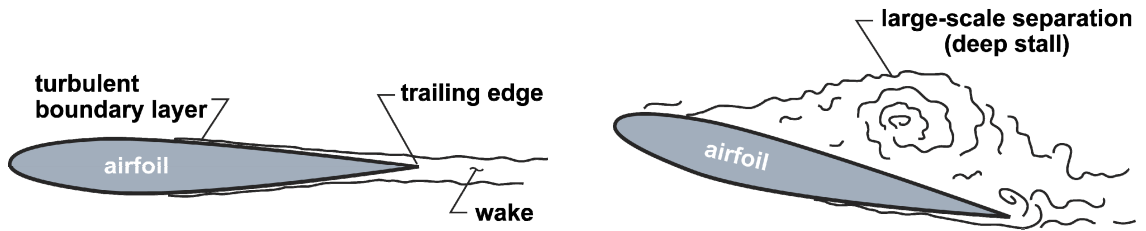


Figure 7: Mechanisms of normal trailing edge noise (left) and stall noise (right) [20]. The larger turbulence length scale for stalled flow results in increased low-frequency noise.

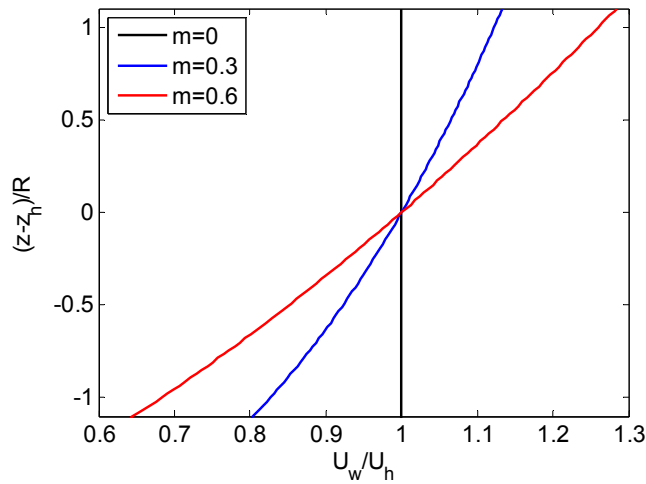


Figure 8: Wind profile in rotor plane for different values of the wind shear factor m .

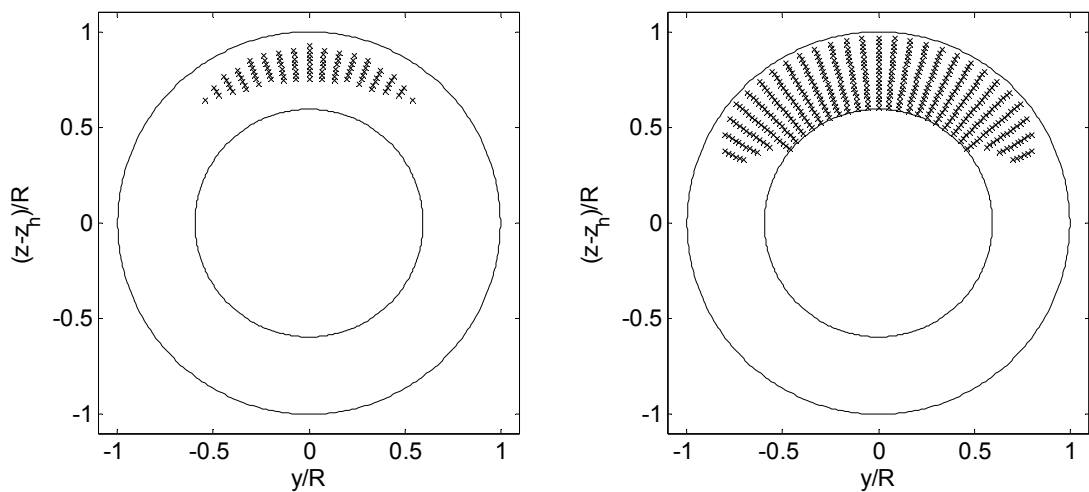


Figure 9: Locations in the rotor plane where stall can occur, for a wind shear factor of 0.3 (left) and 0.6 (right). The circles indicate the outer 40% of the blade.

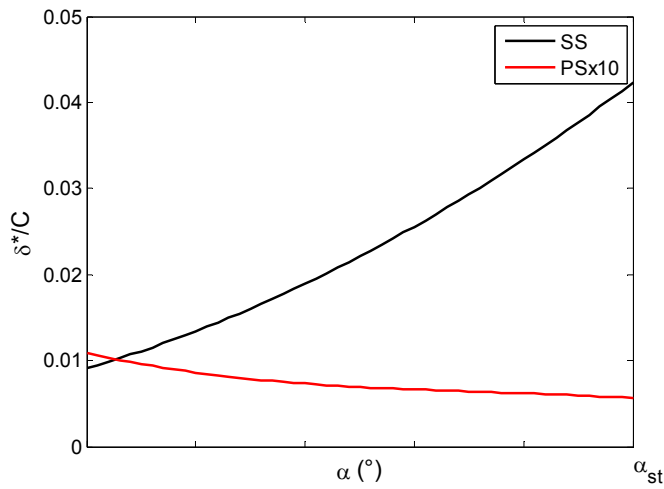


Figure 10: Normalised trailing edge boundary layer displacement thickness as a function of angle of attack, for suction side and pressure side (multiplied by 10). The tick marks on the horizontal axis are spaced at 1°.

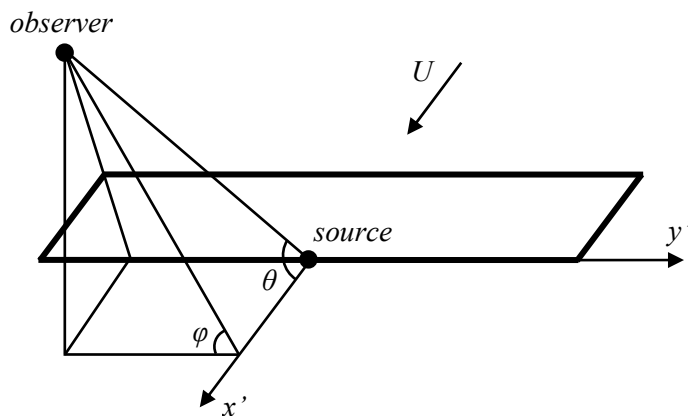


Figure 11: Definition of angles between observer and trailing edge source.

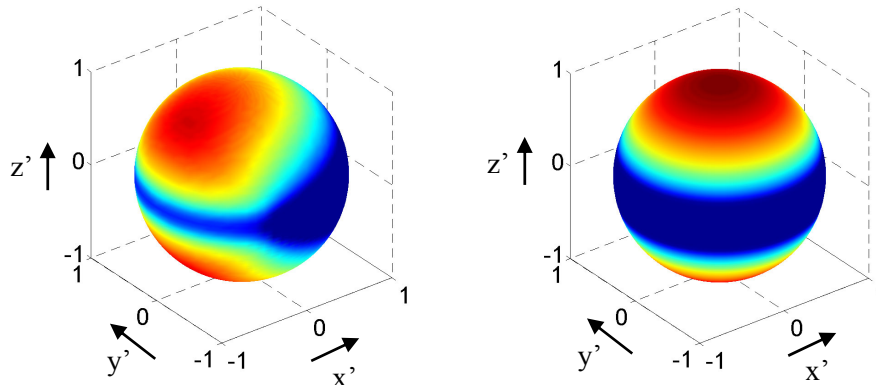


Figure 12: Directivity functions for trailing edge noise (left) and stall noise (right). The source is located at the centre of the sphere. The flow is in the x' -direction and the trailing edge runs along the y' -axis. The range of the color scale is 12 dB.

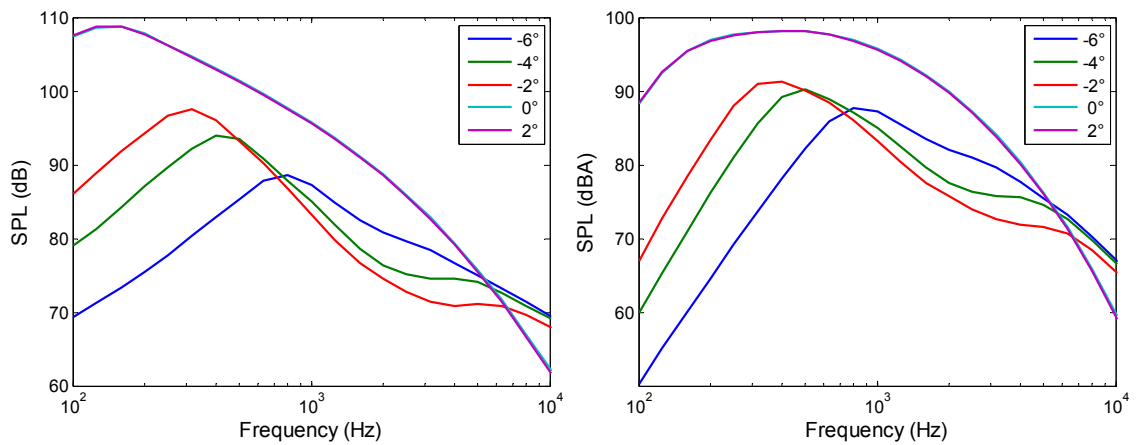


Figure 13: Source spectra for blade section in dB (left) and dBA (right) as a function of relative angle of attack (0° corresponds to the stall angle). The lines for 0° and 2° are practically on top of each other.

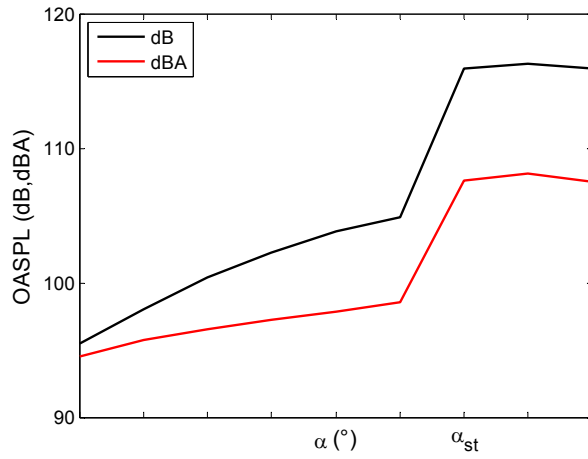


Figure 14: Overall sound level for blade section as a function of angle of attack. The tick marks on the horizontal axis are spaced at 1° .

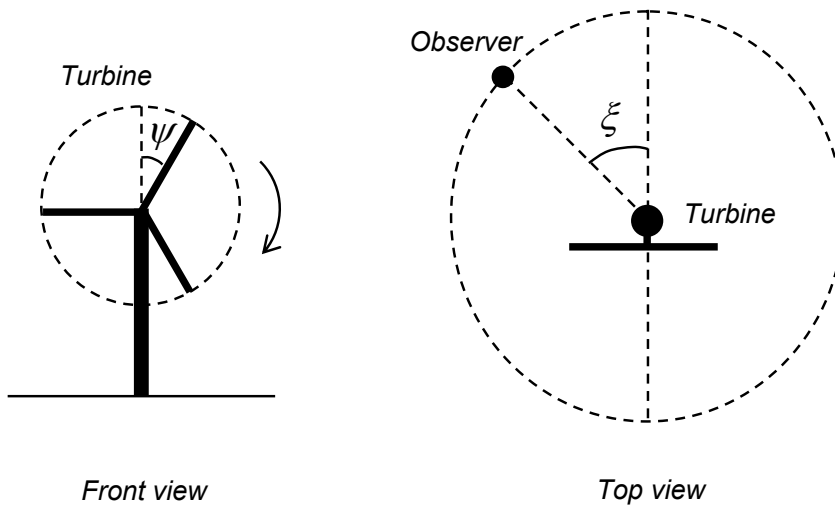


Figure 15: Definition of rotor azimuth angle ψ and observer angle ξ .

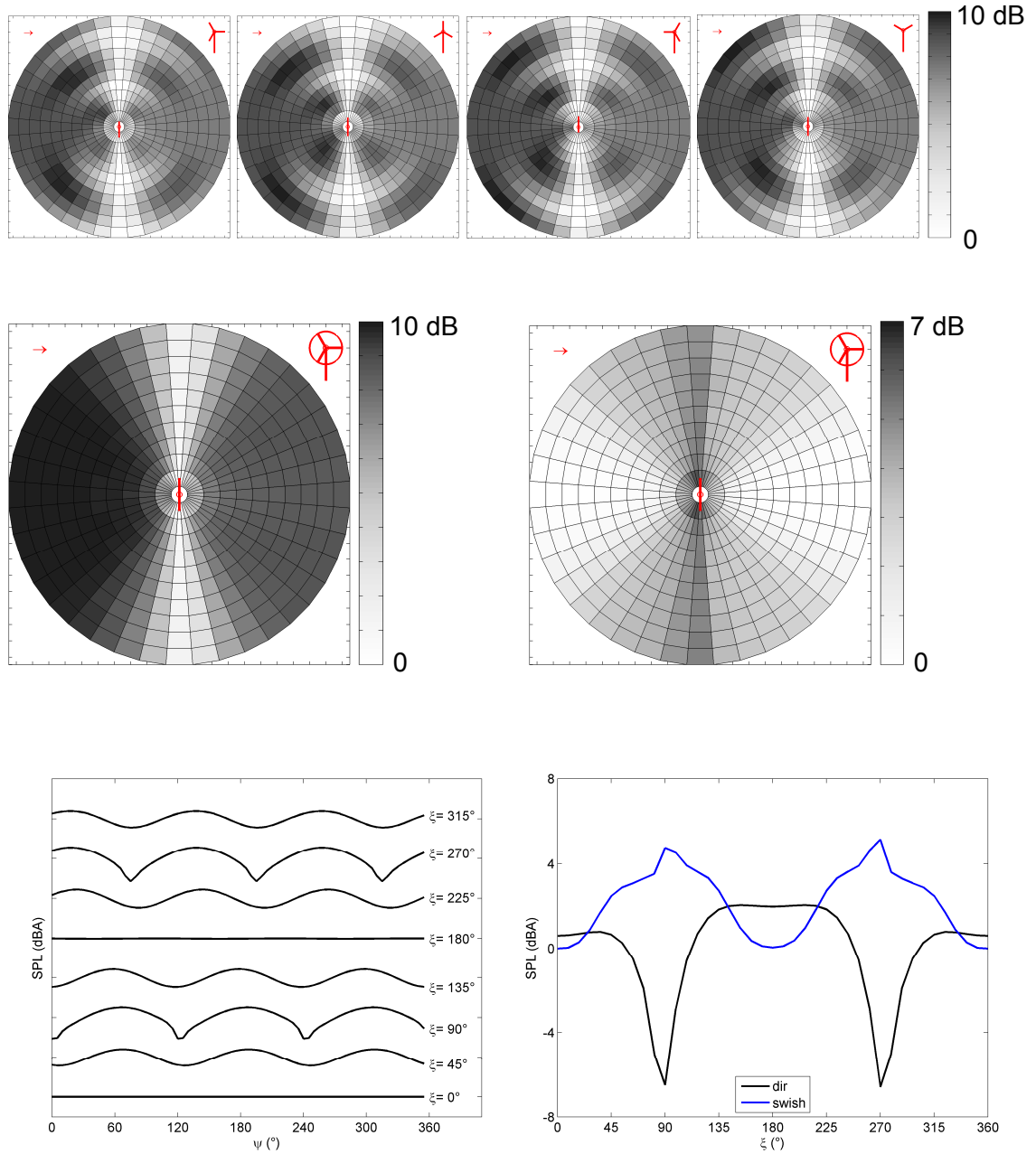


Figure 16: Simulation results for Case 1 ($m=0$, attached flow). Upper row: instantaneous noise footprints. Middle row: average and swish footprint. Lower row: time histories and directivity at large distance (10 rotor diameters from turbine).

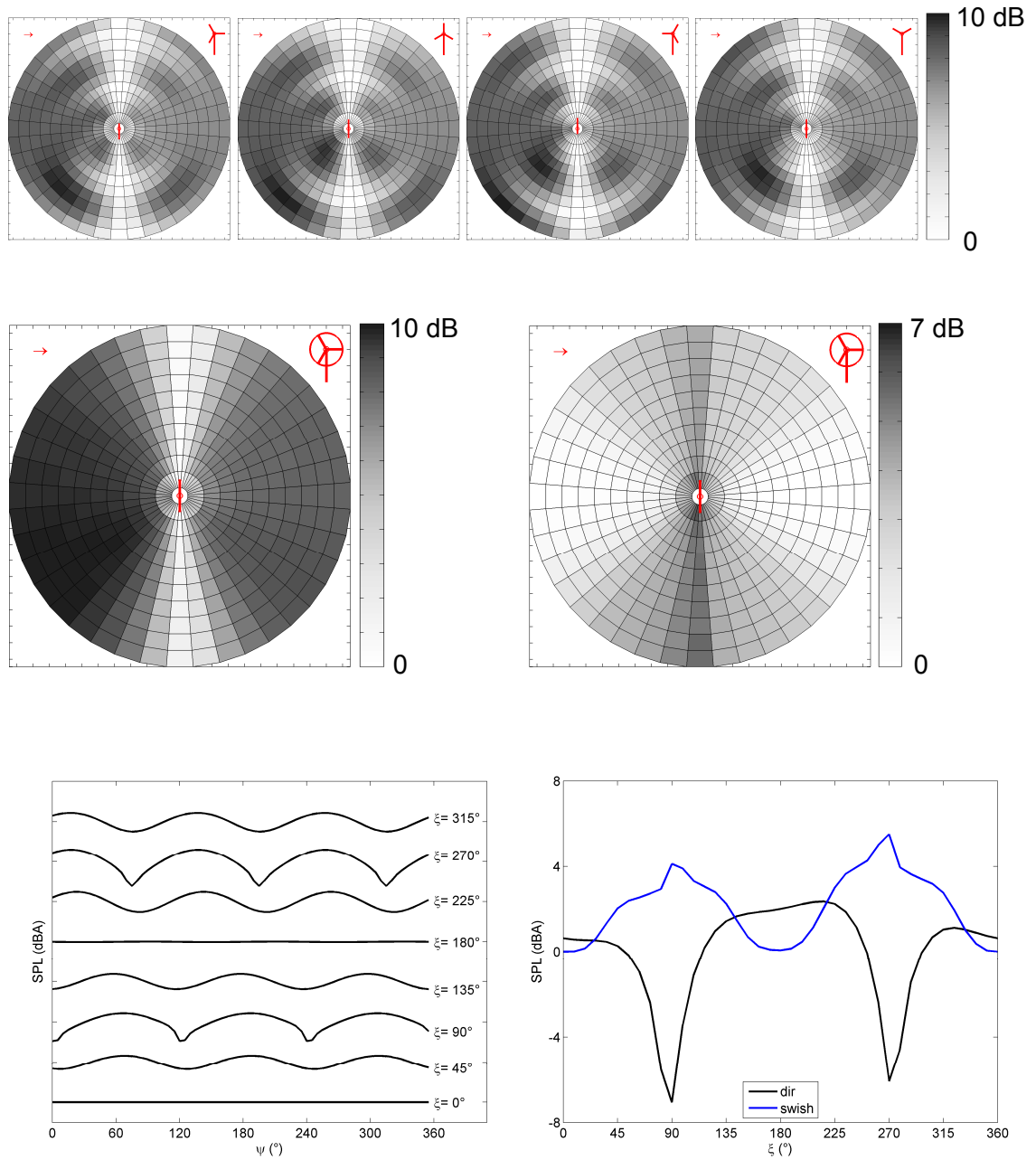


Figure 17: Simulation results for Case 2 ($m=0.3$, attached flow). Upper row: instantaneous noise footprints. Middle row: average and swish footprint. Lower row: time histories and directivity at large distance (10 rotor diameters from turbine).

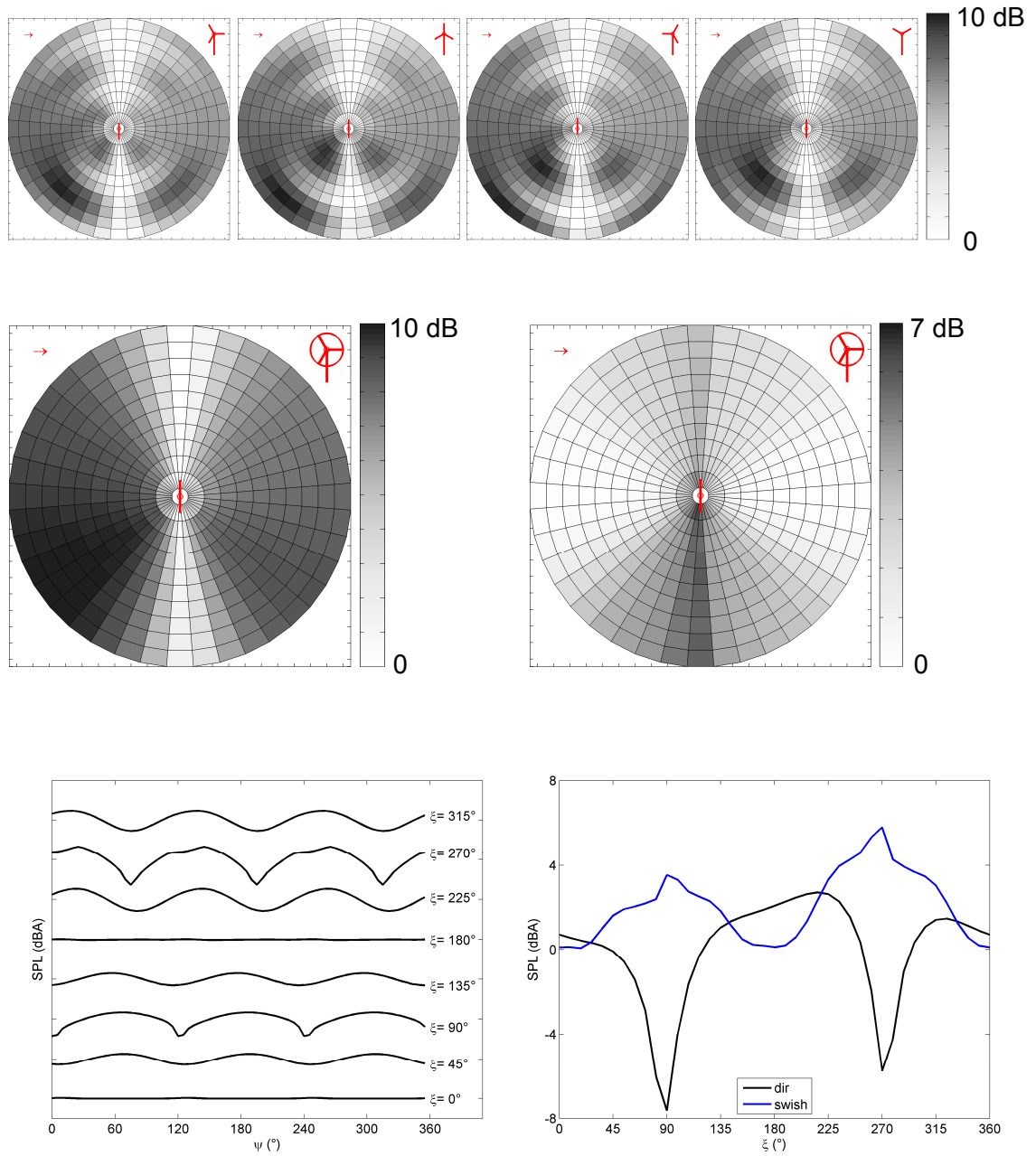


Figure 18: Simulation results for Case 3 ($m=0.6$, attached flow). Upper row: instantaneous noise footprints. Middle row: average and swish footprint. Lower row: time histories and directivity at large distance (10 rotor diameters from turbine).

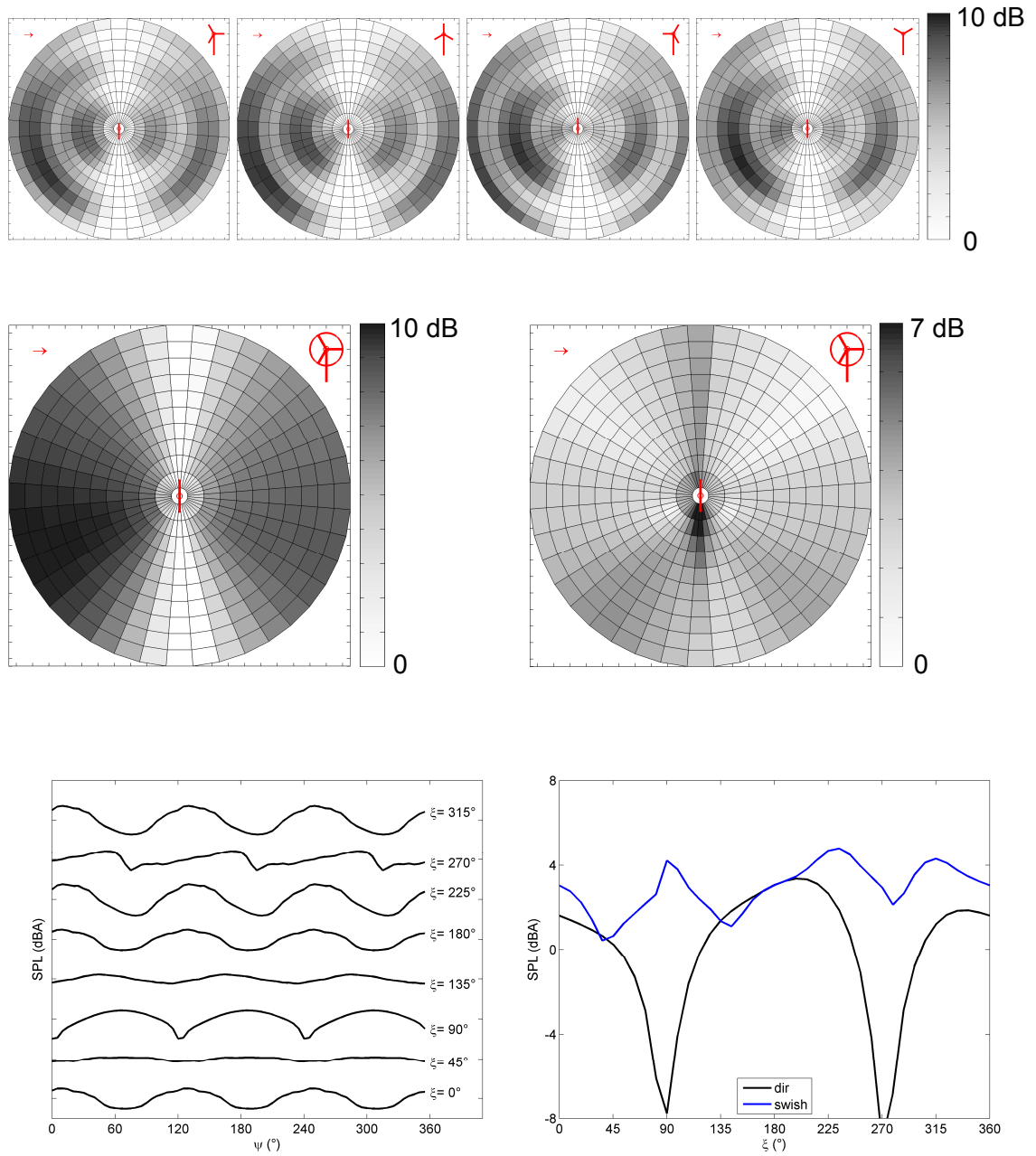


Figure 19: Simulation results for Case 4 ($m=0.3$, local stall). Upper row: instantaneous noise footprints. Middle row: average and swish footprint. Lower row: time histories and directivity at large distance (10 rotor diameters from turbine).

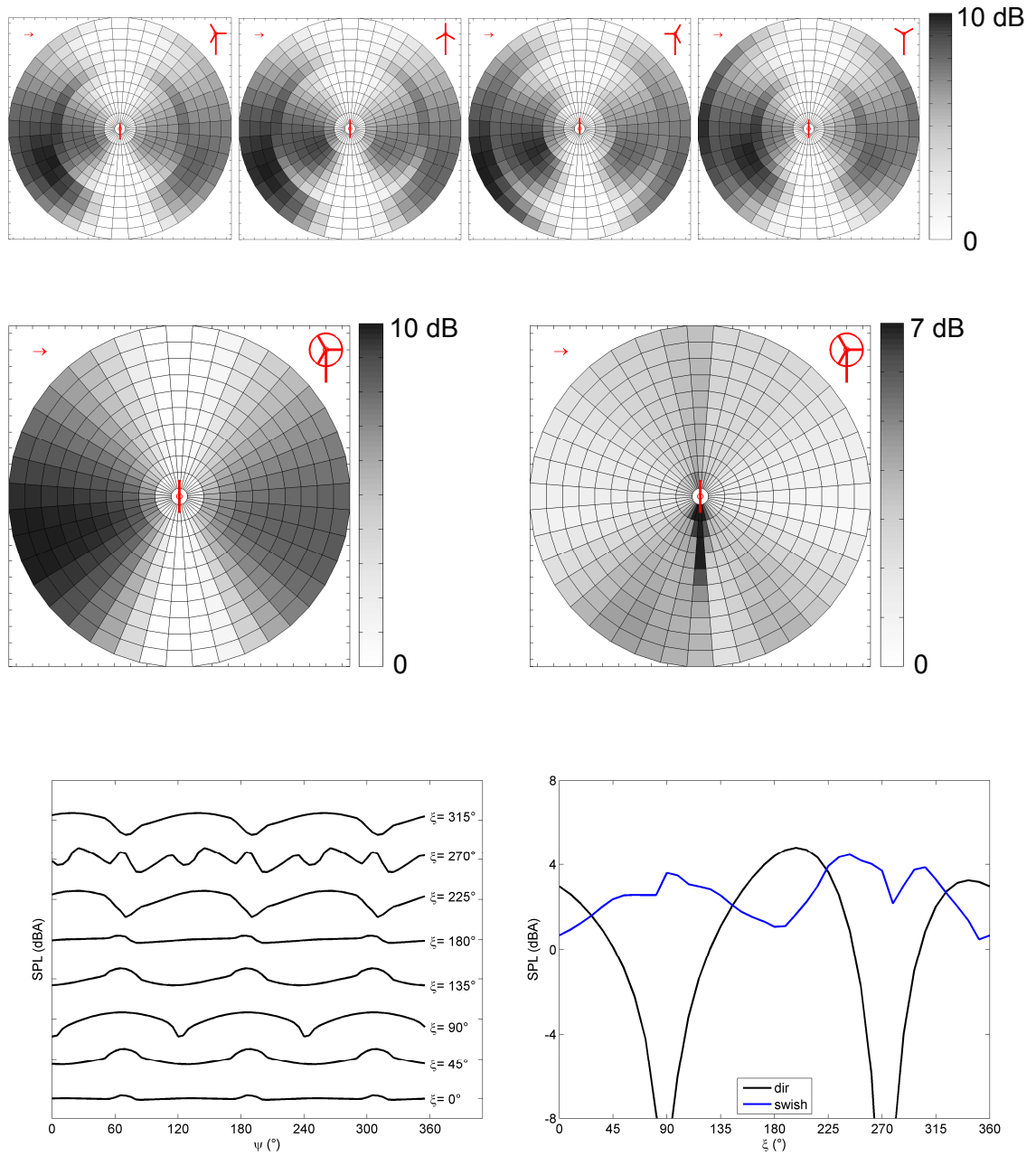


Figure 20: Simulation results for Case 5 ($m=0.6$, local stall). Upper row: instantaneous noise footprints. Middle row: average and swish footprint. Lower row: time histories and directivity at large distance (10 rotor diameters from turbine).

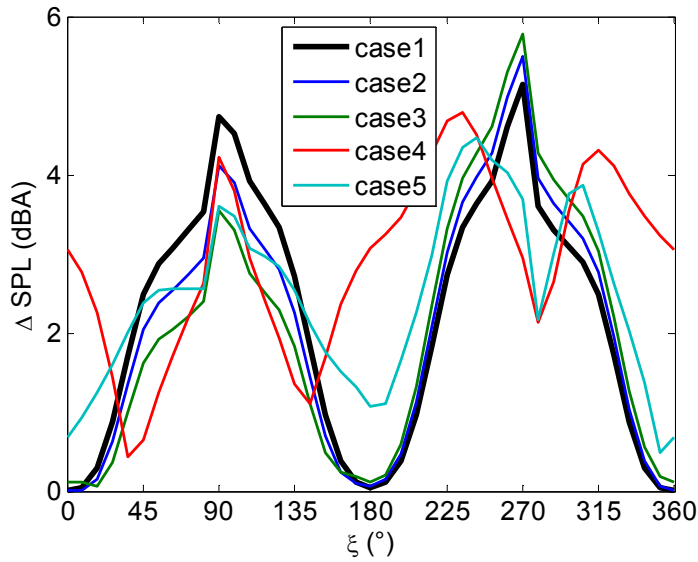


Figure 21: Modulation amplitude at large distance (10 rotor diameters from turbine).

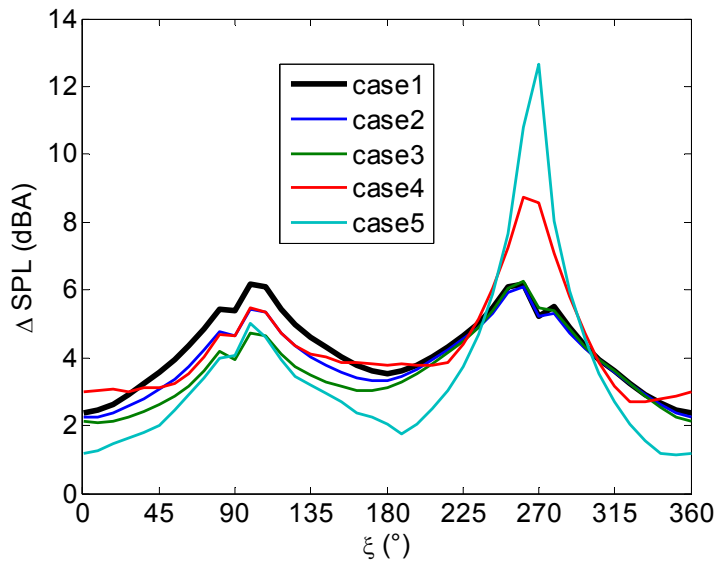


Figure 22: Modulation amplitude at one rotor diameter from turbine.

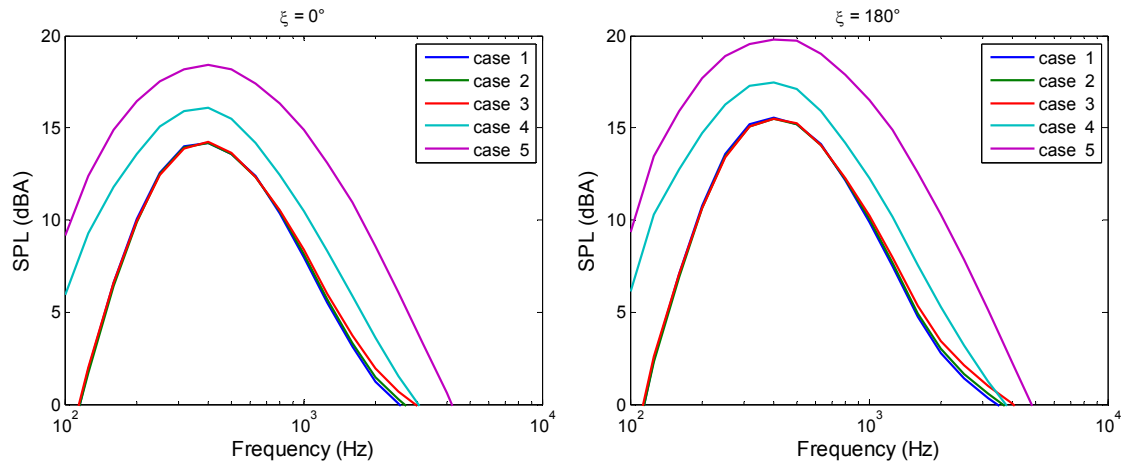


Figure 23: Average spectra for different cases, perceived at large distance (10 rotor diameters from turbine) on a downwind (left) and upwind (right) position.

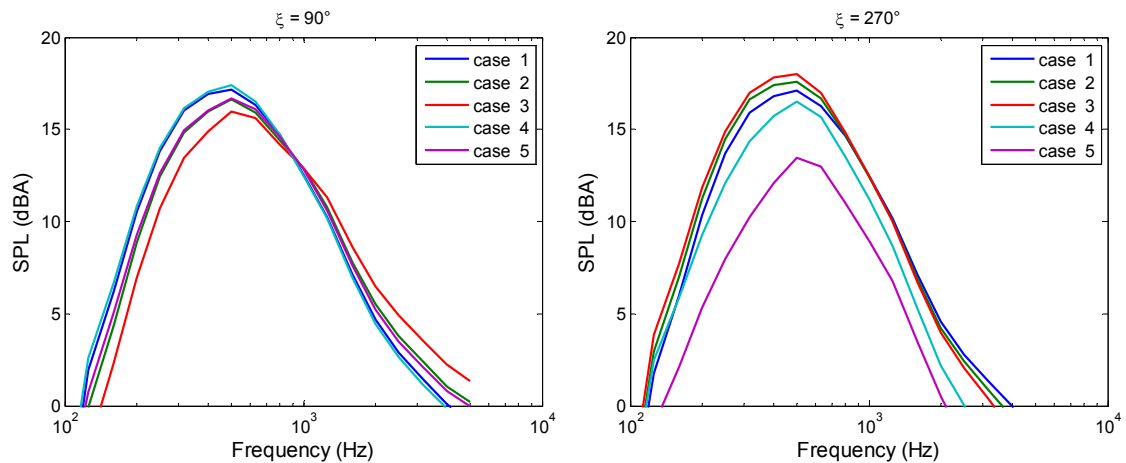


Figure 24: Average spectra for different cases, perceived at large distance (10 rotor diameters from turbine) on both cross-wind positions.

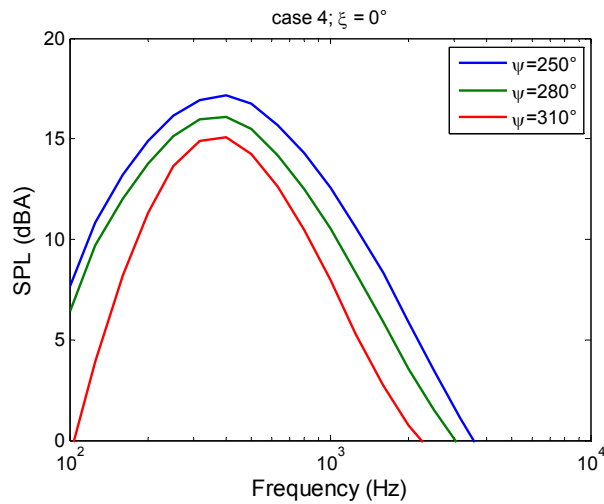


Figure 25: Instantaneous spectra for Case 4, perceived at large distance (10 rotor diameters from turbine) on the downwind position. The blue and red lines correspond to the peak and trough of the modulation (see also Figure 19).

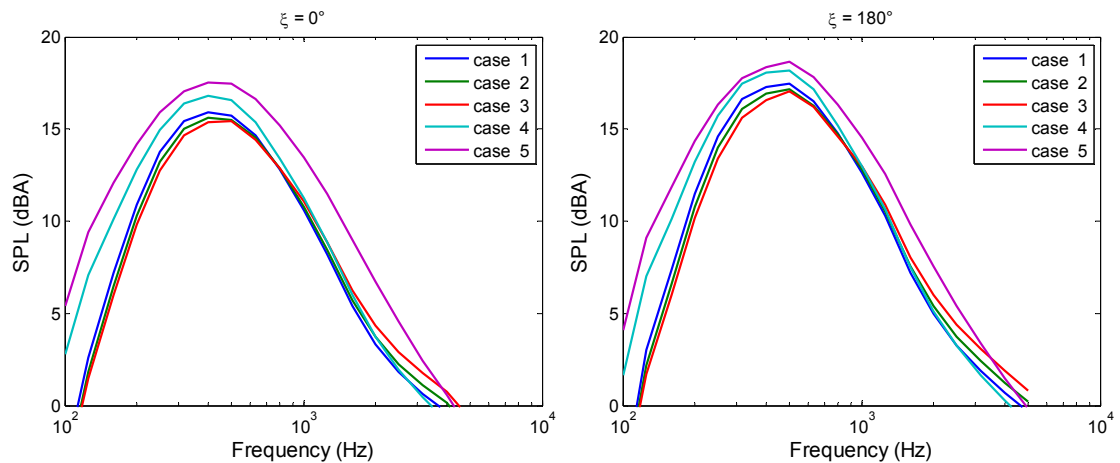


Figure 26: Average spectra for different cases, perceived at one rotor diameter from the turbine on a downwind (left) and upwind (right) position.

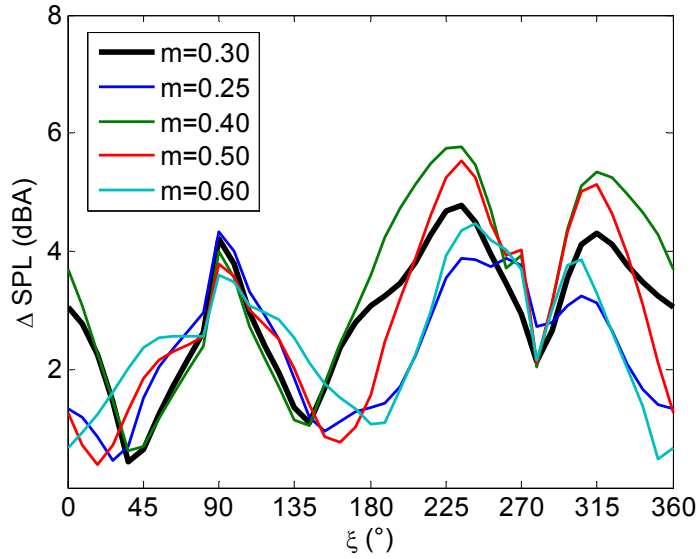


Figure 27: Effect of wind shear exponent on modulation amplitude at large distance (10 rotor diameters from turbine).

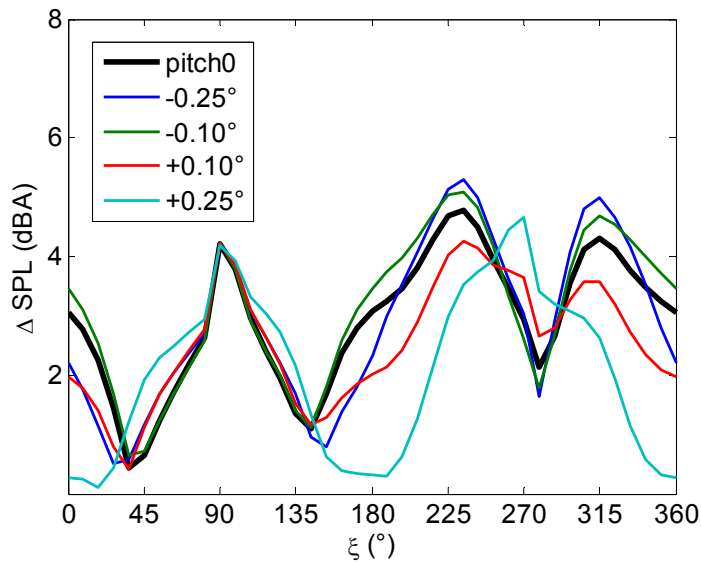


Figure 28: Effect of blade pitch angle on modulation amplitude at large distance (10 rotor diameters from turbine).

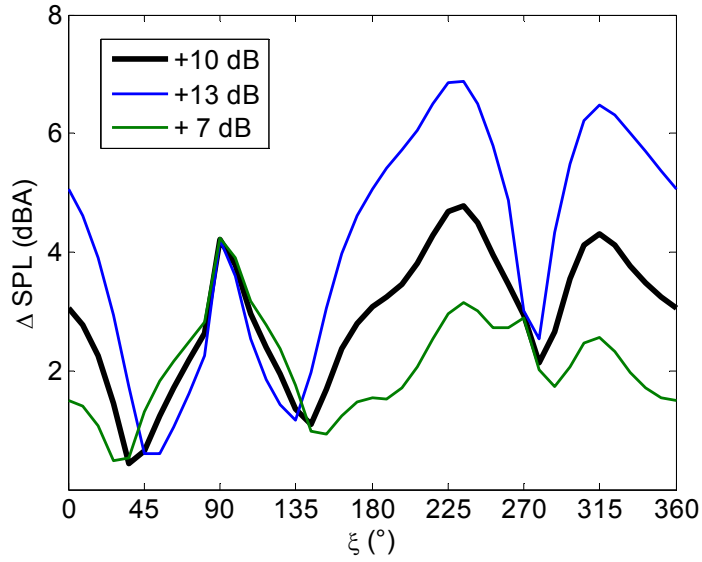


Figure 29: Effect of stall noise level increase on modulation amplitude at large distance (10 rotor diameters from turbine).